NREL/TP-442-6008 • UC Category: 261 • DE94000231

The Identification Of Inflow Fluid Dynamics Parameters That Can Be Used To Scale Fatigue Loading Spectra Of Wind Turbine Structural Components

N. D. Kelley

Prepared for the
13th ETCE Wind Energy Symposium
January 23–26, 1994
New Orleans, Louisiana

National Renewable Energy Laboratory
1617 Cole Boulevard
Golden, Colorado 80401-3393
A national laboratory operated for
the U.S. Department of Energy
under contract No. DE-AC02-83CH10093

Prepared under Task No. WE318010

November 1993

NOTICE

Printed in the United States of America
Available from:
National Technical Information Service
U.S. Department of Commerce
5285 Port Royal Road
Springfield, VA 22161

Price: Microfiche A01
Printed Copy A02

Codes are used for pricing all publications. The code is determined by the number of pages in the publication. Information pertaining to the pricing codes can be found in the current issue of the following publications which are generally available in most libraries: *Energy Research Abstracts (ERA)*; *Government Reports Announcements* and Index (*GRA* and I); *Scientific and Technical Abstract Reports (STAR)*; and publication NTIS-PR-360 available from NTIS at the above address.

THE IDENTIFICATION OF INFLOW FLUID DYNAMICS PARAMETERS THAT CAN BE USED TO SCALE FATIGUE LOADING SPECTRA OF WIND TURBINE STRUCTURAL COMPONENTS

N.D. Kelley
Wind Technology Division
National Renewable Energy Laboratory
Golden, Colorado

ABSTRACT

We have recently shown that the alternating load fatigue distributions measured at several locations on a wind turbine operating in a turbulent flow can be described by a mixture of at least three parametric statistical models [1]. The rainflow cycle counting of the horizontal and vertical inflow components results in a similar mixture describing the cyclic content of the wind. We believe such a description highlights the degree of non-Gaussian characteristics of the flow. We present evidence that the severity of the low-cycle, high-amplitude alternating stress loads seen by wind turbine components are a direct consequence of the degree of departure from normality in the inflow.

We have examined the details of the turbulent inflow associated with series large loading events that took place on two adjacent wind turbines installed in a large wind park in San Gorgonio Pass, California. In this paper, we describe what we believe to be the agents in the flow that induced such events. We also discuss the atmospheric mechanisms that influence the low-cycle, high-amplitude range loading seen by a number of critical wind turbine components. We further present results that can be used to scale the specific distribution shape as functions of measured inflow fluid dynamics parameters.

NOMENCLATURE

c_p = specific heat at constant pressure
g = gravity acceleration
H = vertical heat flux
L = Obukhov length, $-u_{*_o}{}^3 c_p \rho T/gH\kappa$
p = local atmospheric pressure in mb
p_o = reference atmospheric pressure (1000 mb)
Ri = gradient Richardson number, $(g/\Theta)/[(\Delta\theta/\Delta z)/(\Delta U/\Delta z)^2]$
S-N= cyclic stress (S) vs logarithm of N cycles to failure
T = sensible absolute air temperature
u = longitudinal wind velocity component
u_* = local friction velocity at hub height
u_{*_o} = surface layer friction velocity
U_H = horizontal wind speed
v = crosswind or lateral wind velocity component
w = vertical wind velocity component
z = height above local terrain
z/L = expression of atmospheric static stability
β_o, β_1= scaling parameters for exponential distribution
γ_o,γ_1,γ_2 = scaling parameters for extreme value distribution
ξ = Poisson process mean occurrence rate or intensity
κ = von Karman constant (≈ 0.4)
θ = potential temperature, $T(p_o/p)^{.286}$
Θ = layer mean potential temperature
ρ = air density
(') = fluctuating quantity with zero mean

INTRODUCTION

In the development of new turbines, the challenge for the designer is to incorporate sufficient strength in the structural components to *safely* sustain a 20- or 30-year lifetime. To achieve such as design, the designer must have a reasonable understanding of the load and stress distributions that can be expected over the turbine lifetime. Sources of such loads found in the normal operating environment include start/stop cycles, emergency shutdowns, the turbulence environment associated with the specific site and turbine location, and extreme or "rare" events that can challenge the turbine short-term survivability. Episodes that fall into the last category can result from an operational (controller failure) or a violent atmospheric phenomena (tornadic circulations, strong gust fronts, etc.). For the majority of the operating time; however, the character of the turbulent inflow is the dominant source of the alternating stress distributions experienced by the structural components.

The stochastic characteristics of the turbulent inflow are of major significance in influencing the rate accumulation of alternating stress cycles experienced by structural components in wind turbines. We have recently shown that the distributions of these cycles can be described by a mixture of at least three

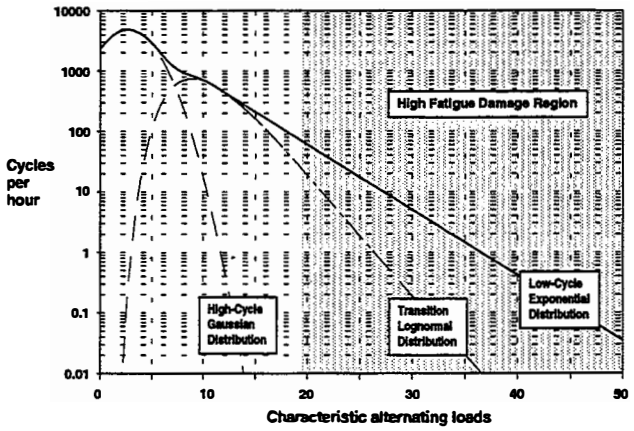

FIGURE 1. SCHEMATIC OF LOADING CYCLE RANGES AND MIXED DISTRIBUTION MODEL

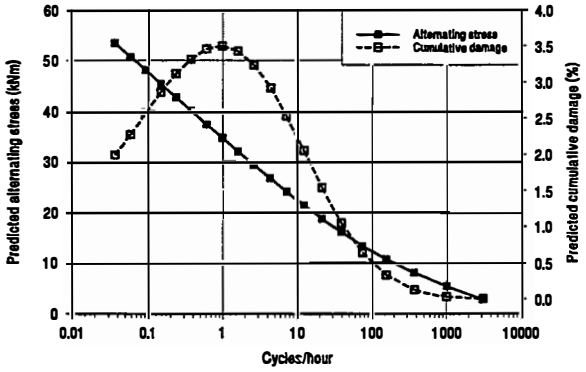

FIGURE 2. PREDICTED REGION OF HIGH FATIGUE DAMAGE FOR STEEL MAIN SHAFT (*after Jackson [4]*)

parametric statistical models [1-3]. The rainflow counting of the turbulent wind components has that shown a similar mixture can be used for describing their cyclic content. The non-Gaussian nature of the flow and turbine response is underscored by the inclusion of the lognormal and exponential models in the distribution mixture. Figure 1 diagrammatically compares the contributions of the Gaussian, lognormal, and exponential models to the mixture.

Recent analyses of the loading events associated with turbine rotor blades constructed of composite materials have shown that the majority of the fatigue damage is associated with events occurring at a comparatively low occurrence (low-cycle) rate but with high amplitudes. We will subsequently refer to this low-cycle, high-amplitude range as the *LCHA*. This is particularly true of blade materials that are characterized by a high S-N exponent. As an example, a recent analysis of the predicted fatigue damage associated with the bending of a turbine low-speed shaft by Jackson [4] is presented in Figure 2. While the material of concern here was steel (S-N exponent of -0.092), the peak contribution to the predicted fatigue damage was clearly in the LCHA (1 cycle/h) range. The plot of the predicted shaft alternating stress spectrum clearly shows the deviation from the exponential model at frequencies greater than about 10/h.

In this paper, we will present what we believe to be efficient and justifiable parametric distribution models for the LCHA alternating stresses accumulated as a result of turbulent forcing. We discuss the role of two atmospheric fluid dynamics parameters that influence the scaling of the parametric models and therefore the fatigue load distribution spectra that can be expected. Though these conclusions were reached from data collected in a rigorous wind park environment, we believe the concept to be universal since these parameters can be measured in any operating environment. We also offer a brief discussion of the probable atmospheric mechanisms that are ultimately responsible for the observed load distributions in a specific operating environment.

APPROACH

Our methodology has been to

- Establish the sample population distribution of a range of turbine dynamic parameters by summing the rainflow cycle counts from 405 individual, 10-minute records and by rainflow counting them concatenated into a single record 67.5 h in length
- Compare the sample population distributions using both methods and justify the results
- Determine an appropriate parametric distribution and boundaries for the low-cycle, high-amplitude alternating cycle range normalized to one hour
- Fit the observed distributions to the appropriate parametric model and determine the corresponding model scaling parameters
- Repeat the previous steps on a series of twelve categorical sub-populations of 10-minute records which have been classified by the mean atmospheric stability (Richardson No., Ri) and hub-height horizontal wind speed ($\overline{U_H}$)
- Using Analysis of Variance (ANOVA) techniques, identify the most efficient predictors of the cycle distribution model scaling parameters from a range of measured fluid dynamics parameters related to the turbulent inflow
- Discuss the atmospheric mechanisms that are most likely to be responsible for influencing shape and occurrence of the observed alternating load distributions.

ALTERNATING CYCLE DISTRIBUTION MODELS

The measurements used to determine the sample population alternating load distributions were derived from the simultaneous testing of two adjacent Micon 65/13 turbines in a large wind park in San Gorgonio Pass, California. The Micon 65/13 is a stall-regulated, three-bladed, upwind turbine with a rigid hub and an active yaw drive. Both turbines were identical except that one had a rotor based on the NREL (SERI) Thin-Airfoil Family and the other was an original AeroStar design. Various NREL docu-

TABLE 1

Parameter	10-min sum record β_1 (± 95% Conf Limits)	Single record count β_1 (± 95% Conf Limits)	10-min sum Return Rate (h)	Single record Return Rate (h)
root flapwise moment w/1.1 kNm resolution	– 0.2780 **–0.2759** – 0.2738	– -0.2782 **–0.2761** – 0.2740	823 @ 55 kNm	830 @ 55 kNm
root flapwise moment w/2.67 kNm resolution	– -0.2988 **–0.2960** – 0.2932	– 0.2919 **–0.2887** – 0.2855	712 @ 55 kNm	539 @ 55 kNm
	γ_2	γ_2		
root edgewise moment w/0.6 kNm resolution	1.4522 **1.3624** 1.2726	1.4527 **1.3629** 1.2731	9.4 @ 30 kNm	9.4 @ 30 kNm
root edgewise moment w/2.67 kNm resolution	1.4453 **1.4426** 1.4399	1.4495 **1.4455** 1.4415	5.4 @ 30 kNm	5.3 @ 30 kNm

ments [1,3,5] discuss the experiment in more detail. The rainflow cycle counting was performed using a slightly modified version of the so-called "single" pass algorithm of Downing and Socie [6]; in which all open half-cycles are closed. See Sutherland and Butterfield [7] for a more complete discussion. Dynamic loads from a range of turbine structural components that are of interest to the designer were analyzed. These loads included the blade root flapwise and edgewise bending moments, low-speed shaft torque and bending moments, yaw drive torque, axial and inplane thrust measured at the nacelle, axial and inplane thrust measured on the tower, and tower axial and inplane bending.

Parametric Model Identification

Each of the above turbine dynamics was rainflow counted using each of the 405 individual 10-minute records and then the results were summed as well as by counting the series concatenated as a single record 67.5 h long. An examination of the resulting sample population distributions revealed that, except for the root edgewise bending moment, the LCHA range of the remaining parameters could be described very accurately with an asymptotically decaying *exponential distribution*. It was found that the range of this exponential distribution extended up to a frequency of about 100 cycles/h. For re-occurring events at frequencies greater than 100 cycles/h or periods shorter than about 2 minutes (in the lognormal transition region), the deviation from the exponential model becomes significant. For the edgewise bending moment, an *extreme value distribution (Type I)* was found to best fit the observed population. The pertinent distribution parameters for the exponential distribution are the amplitude (β_0) and the shape factor (β_1) (usually referred to as the slope or rate), whose density function is given by

$$N = \beta_0 e^{-\beta_1 M_{p\text{-}p}} \qquad (1)$$

where N is the number of cycles per hour and $M_{p\text{-}p}$ is the peak-to-peak value of the moment. The parameters for the extreme value distribution include the scale or amplitude (γ_0), the position (γ_1), and the width or shape (γ_2) and whose density function is expressed as

$$N=\gamma_0 \exp\left[-\exp\left[-\left(\frac{M_{p\text{-}p}-\gamma_1}{\gamma_2}\right)\right]-\left(\frac{M_{p\text{-}p}-\gamma_1}{\gamma_2}\right)+1\right]. \qquad (2)$$

Concatenated Versus 10-minute Record Summation Rainflow Counting Results

We noted that the loads from each blade on both turbines differed with one significantly more active than its companions. The reason this occurred is still not clear. Because only one blade on each rotor was involved, we have speculated there may have been a systematic misalignment in the hub configuration of each machine. Given this, we have used the mean of the three-blade distributions of the flap- and edgewise loads to better understand the underlying physical process. In Table 1, we summarize the important measured distribution shape or width (β_1 and γ_2) parameters for these loads and their 95% confidence limits using the NREL rotor. This table contains the results from both the summation of individual 10-minute records and the concatenated time series. It also includes the impact of the resolution used in calculating the rainflow histograms (2.67 vs 1.1 kNm flapwise resolution for example). This table shows that by summing the rainflow matrices derived from a population of 10-minute records, little is lost when compared to a concatenated record of the same length. There is some non-conservative behavior with respect to resolution which suggests a resolution of about 1 kNm is appropriate. The estimated re-occurrence or return rates of loads outside the observed range vary by less than a factor of two indicating that the extrapolation of these results should be conservative.

Physical Interpretation of Parametric Models

We believe that the observed asymptotic behavior of the LCHA load range in all of the measured dynamic parameters is a consequence of the accumulation or *counting* of cycles formed by the process of joining of two stochastic events: a *peak* and a *valley in the load history*. Following Roth [8], such a process is known as a "counting" process if $N(\Delta t)$ represents the number of events occurring in the interval Δt. The process is considered *Poisson* if it has a mean (constant) rate (of occurrence) ξ, where $\xi > 0$. Further stipulations include that the events occur independently of one another, the number of observed events in Δt depends only on the length of Δt (stationarity), and the number of events in Δt is Poisson distributed with mean $\xi\Delta t$. In our case, an "event" is defined as the closing of a stress/strain hysteresis loop taking place within a specified counting interval Δt. Our observation, that at intervals exceeding 1.67 minutes (100 cycles/hour) the distribution of load cycles is exponential, is consistent with a Poisson process. At intervals less than about 2 minutes, the

TABLE 2

Stability Class	Wind Speed Class	N (recs)	$\overline{U_h}$ (ms^{-1})	$\overline{\sigma_h}$ (ms^{-1})	$\overline{TI}$	$\overline{Ri}$	Median Hub Reynolds Stress Components (ms^{-1})		
							$\overline{(u'w')}^{1/2}$	$\overline{(u'v')}^{1/2}$	$\overline{(v'w')}^{1/2}$
2U	3	7	5.90	1.655	0.28	–0.216	0.562	0.192	0.474
2U	4	28	7.55	1.974	0.26	–0.092	0.755	0.497	0.447
2U	5	45	9.44	2.503	0.26	–0.040	0.939	0.436	0.436
2U	6	12	11.22	2.749	0.25	–0.005	1.132	0.917	0.720
3N	5	6	9.91	2.522	0.25	+0.006	1.072	0.525	0.492
3N	6	28	11.43	2.776	0.24	+0.005	1.210	0.657	0.578
3N	7	10	13.14	2.883	0.22	+0.007	1.346	0.396	0.652
4	4	23	7.86	2.125	0.27	+0.075	0.867	0.791	0.630
4	5	77	9.78	2.457	0.25	+0.038	1.079	0.675	0.641
4	6	99	11.44	2.714	0.24	+0.033	1.251	0.841	0.629
4	7	63	13.08	2.887	0.22	+0.022	1.411	0.801	0.638
4	8	5	14.75	2.690	0.18	+0.012	1.503	0.863	0.715

fluctuating loads reflect some temporal coherence. This is consistent with our measurements of the turbulent integral time scales of the three wind components shown in Figure 3. Within the wind park environment and for periods exceeding 2 minutes, the interval between cycle closures (events) is observed to be exponentially distributed with scale β_1. If the observation period, Δt, is sufficiently short to ensure stationarity, then the number of cycles occurring in that period is Poisson distributed with a mean rate of occurrence or intensity function $1/\beta_1$ and Poisson mean $\Delta t/\beta_1$. The probability that exactly n cycles will be counted in the LCHA range during the period Δt is

$$P(N=n)=\frac{(1/\beta_1)^n}{n!}e^{-1/\beta_1}. \quad (3)$$

If the observational period Δt is too long to achieve at least quasi-stationarity, then we must assume a *nonhomogenous* Poisson process

$$P(N=n,t)=\frac{(1/\beta_1(t))^n}{n!}e^{-1/\beta_1(t)}. \quad (4)$$

We must now define relationships between the intensity function, $1/\beta_1$, and fluid dynamics parameters of the inflow which are themselves functions of time.

While all the turbine alternating load distributions can be described by Eq.(1) in the LCHA range, the root edgewise bending in its raw form cannot. The edgewise signal is unique in that it contains a strong sinusoidal component arising from the gravity load modulating the more random turbulence-induced loads. Sutherland and Osgood [9] have suggested removing the deterministic gravity signal from the edgewise time series by subtracting a sinusoid derived from azimuth averaging. This approach is only appropriate if the rainflow counting is applied off-line where multiple passes through the time series are possible. Instead, we would prefer to apply a methodology that can accommodate on-line rainflow counting of the raw signals in the field for long-term monitoring purposes. The double exponential form of Eq.(2) suggests that some form of a complex modulation of the turbulence-induced and gravity signals, through potential non-linearities, may not be completely distinct. For now, we have elected to continue to describe the LCHA region of the blade edgewise loads using the extreme value distribution with the intent to pursue a less heuristic approach in the future.

IDENTIFICATION OF INFLOW SCALING PARAMETERS

Data Classifications

To identify efficient predictors of the shape (intensity) parameters of the LCHA exponential and extreme value distributions, we categorized the sample population of 10-minute records

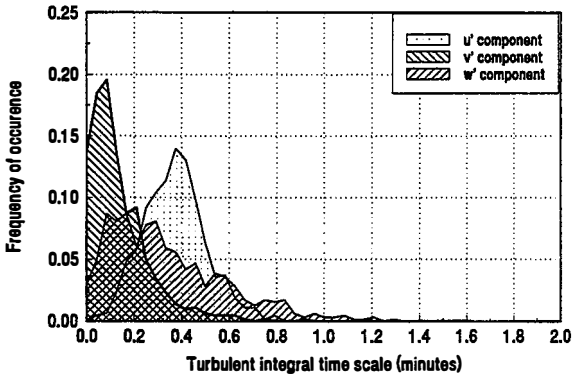

FIGURE 3. OBSERVED TURBULENCE TIME SCALES

TABLE 3

Turbine Dynamic	Statistical Model	Scaling Parameter β_1	
		Dominant Inflow Parameter(s)	*Percent Variance Explained*
Root flap bending moment	exponential	$\overline{(u'w')}^{1/2}$	89
Low-speed shaft torque	exponential	$\overline{(u'w')}^{1/2}$, Ri	78
Low-speed shaft bending	exponential	$\overline{(u'w')}^{1/2}$	94
Yaw drive torque	exponential	$\overline{(u'w')}^{1/2}$, $\overline{(u'v')}^{1/2}$, Ri	87
Tower top torque	exponential	U_H, $\overline{(u'w')}^{1/2}$	88
Tower axial bending	exponential	σ_H	78
Tower inplane bending	exponential	U_H, $\overline{(u'v')}^{1/2}$	82
Nacelle axial thrust	exponential	$\overline{(u'w')}^{1/2}$, $\overline{(u'v')}^{1/2}$	51
Nacelle inplane thrust	exponential	σ_H, Ri	77
Tower axial thrust	exponential	$\overline{(u'w')}^{1/2}$, Ri	62
Tower inplane thrust	exponential	$\overline{(u'w')}^{1/2}$, $\overline{(u'v')}^{1/2}$, $\overline{(v'w')}^{1/2}$, Ri	69
		γ_2	
Root edge bending moment	extrm value	$\overline{(u'w')}^{1/2}$, $\overline{(v'w')}^{1/2}$	86

by first atmospheric stability (Richardson number, Ri) and then by the hub-height mean wind speed, $\overline{U_H}$. Three stability classifications are used: *unstable* (Class 2U, Ri < 0); *near-stable* (Class 3N, 0 ≤ Ri < 0.01); and *stable* (Class 4, Ri ≥ 0.01). The mean wind speed is classified into 2-ms^{-1} categories whose value is approximately one-half of the interval width in meters per second. A total of twelve sub-categories were defined. In addition to the stability and mean wind speed, a series of mean turbulence fluid dynamics parameters were calculated for each sub-category, including the horizontal wind speed standard deviation (σ_H) and turbulence intensity (TI = $\sigma_H/\overline{U_H}$). Because of the character of the distributions, the medians of the hub-level Reynolds stress, $\left(\overline{u_i u_j}\right)^{1/2}$, were included instead of their means. Table 2 summarizes the values of each of these parameters for each category with the number of 10-minute records contained within each.

Sensitivities of Model Scaling to Fluid Dynamics Parameters

The 10-minute record rainflow count spectra for each of the turbine dynamic parameters associated with the sub-categories listed in Table 2 were summed, and the corresponding model scaling parameters, β_1 and γ_2, were calculated for the LCHA region. Each of the shape parameters were then correlated with the inflow dynamic parameter matrix of Table 2 using analysis of variance (ANOVA) techniques. The dominant sensitivities to the latter were identified with their degree of explained variance and are summarized in Table 3. An examination of this table will reveal a strong sensitivity to the vertical momentum transfer, $\left(\overline{u'w'}\right)^{1/2}_{hub}$ or local $-u_*$ and the Ri. The occasional appearance of the other components of the shear stress, $u'v'$ and $v'w'$, shows a sensitivity to *coherent* structures in the flow.

The sensitivity of the β_1 and γ_2 shape parameters as a function of the $u'w'$ component of the mean shear stress for the flap- and edgewise root bending moments on each of the two turbines are presented in Figures 4 and 5. Figure 4 shows a strong trend to a smaller value of β_1 or an increase in mean occurrence rate or intensity ($\xi = 1/\beta_1$) in the LCHA region with increasing shear stress or vertical momentum transfer. The increased sensitivity of the NREL rotor over its counterpart most likely results from several factors. These include its greater swept area, higher aerodynamic activity levels, and because it was operating further into the post stall region when the mean shear stress levels were at their highest. Figure 5 confirms that the shape of the LCHA region for the root edgewise moments is strongly correlated with the inflow turbulence conditions. The sensitivity to increasing mean shear stress levels is high and essentially the same for both rotors.

There is a strong correlation between the stability and the value of u_* as predicted by surface boundary layer theory. The stability parameter used in boundary layer turbulence scaling is the ratio of the height, z, to the Obukhov length scale, L, or z/L (known as the Monin-Obukhov or M-O stability parameter). This parameter is related to Ri. It is identical to Ri for unstable flows (0 < Ri, z/L) but increases more rapidly with increasing positive stability (Ri, z/L ≥ 0) as compared with the value of Ri. This is useful when studying the sensitivity of turbulence scaling in flows that are just slightly stable. We use z/L as the abscissa and plot the mean values of the hub u_* and the β_1 and γ_2 shape parameters for the flap- and edgewise LCHA regions on the right hand ordinate in Figures 6 and 7, respectively. The dotted line in these figures traces a locally regressed, best-fit line for the value

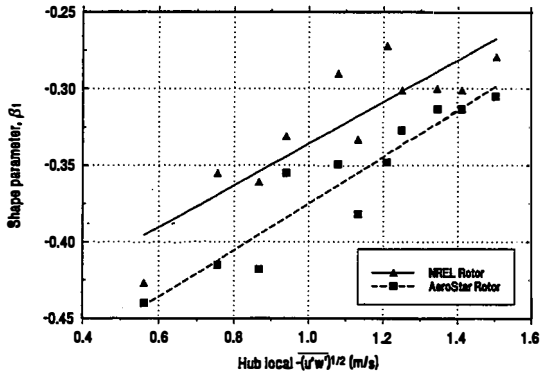

FIGURE 4. SENSITIVITY OF β_1 SHAPE PARAMETER FOR ROOT FLAPWISE LOADS

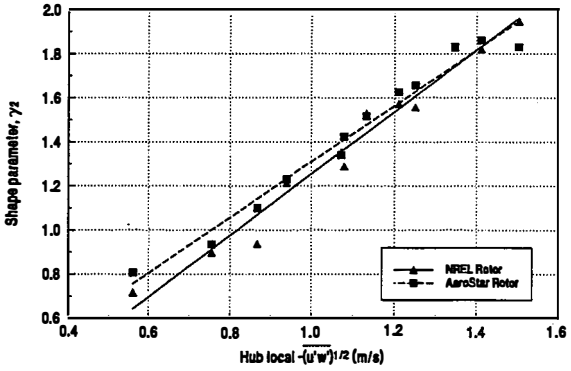

FIGURE 5. SENSITIVITY OF γ_2 SHAPE PARAMETER FOR ROOT EDGEWISE LOADS

of $-\left(\overline{u'w'}\right)^{1/2}$. There is a region of z/L values between about 0.005 and 0.040 in which there is a maximum of vertical momentum transfer and turbulence generation because of the mean high shear stress. Figures 6 and 7 also show that the LCHA regions associated with the flap- and edgewise alternating loads are the *broadest* in this stability range. This means that a wide spectrum of load cycles can occur under such conditions compared with regions to the left or right.

Previously in Figure 1 and in Ref. [3], we hypothesized that the encountering of *coherent turbulent structures* was responsible for the LCHA region of the alternating load spectra. Using the left ordinate of Figure 8, we have plotted the observed normalized cross-covariances or correlation functions for the three turbulent wind components, $\left(\overline{u_i u_j}\right)/\sigma_i\sigma_j$. Using the right ordinate, we have plotted the value of the 25 largest root flapping moments experienced by the NREL rotor on the Micon 65. We also have included the single, largest flap peak seen on the AeroStar rotor. It is clear from Figure 8 that (1) *all* of the extreme peak flap loads occurred in stable flows and (2) the majority occurred during periods when *the flow was dominated by highly correlated or coherent structures*.

ATMOSPHERIC MECHANISMS RESPONSIBLE FOR INFLUENCING LOAD DISTRIBUTIONS

Figures 6 through 8 clearly show the narrow stability range in which strongly coherent flows are common. This range is characterized by the strong vertical transfer of momentum and high three-dimensional mean shear stresses indicating the efficient transfer of energy from the mean flow into turbulence. The LCHA regions of the alternating load spectra broaden in this range indicating a one-to-one correspondence. Any region within a stably-stratified flow in which locally the Ri falls below +0.25 can experience *dynamic instability* [10,11]. This means that under such conditions, small-scale disturbances will grow *exponentially* with time instead of decaying or possibly remaining stable. Because the entire layer between 3 and 31 m was less than the critical Ri value, there is an excellent chance that the conditions for dynamic instability are present within the layer occupied by the wind park turbine rotors. Such conditions are ideal

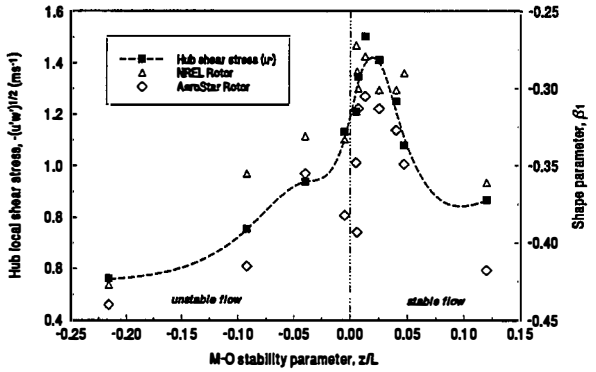

FIGURE 6. VARIATION OF HUB-LEVEL SHEAR STRESS AND FLAPWISE MOMENT β_1 VS STABILITY

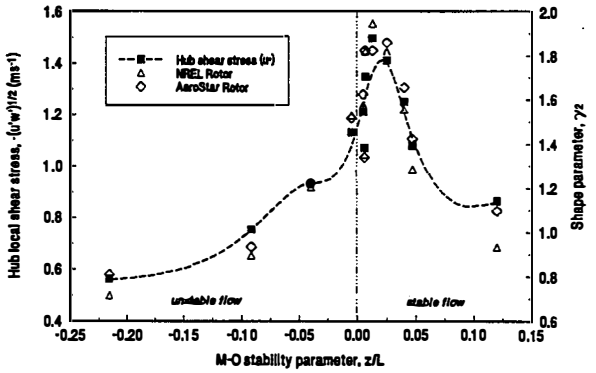

FIGURE 7. VARIATION OF HUB-LEVEL SHEAR STRESS AND EDGEWISE MOMENT γ_2 VS STABILITY

for generating internal gravity waves and various forms of transient shear-generated phenomena such as Kelvin-Helmholtz (KH) instabilities. The latter are characterized by regions of strong vorticity and highly coherent turbulence.

We suspect that under the conditions listed above, dynamic instability does exist within the layer defined by the park turbine rotors, and the discharge of the turbine wakes into this unstable layer causes them to become more intense with time rather than decay. An analysis of the conditions surrounding the occurrence of the peak flapping loads on the NREL-equipped turbine has revealed that they occur only over a small portion of the rotor disk. Figure 9 displays the disk coordinates where two of the largest observed flapwise peaks originated. Case A of Figure 9 took place in a less stable flow (z/L = +0.007) than that of Case B (the largest observed load peak), in which z/L = +0.041. The polar plots of Figure 9 represent 5 seconds of data surrounding the extreme event. The peak phenomena show up on all three blades and occupy 30° or less of the disk. The equivalent linear distance traversed is in the range of 3-4 m. The order in which the blades encountered the disturbances (1,3,2 for Case A and 2,1,3 for Case B) indicates that the disturbances were moving vertically as well as horizontally through the disk. The effect of stability is also evident when comparing the character of the polar plots of Cases A and B. In Case A, the loading pattern is skewed to the upper right quadrant and the region of enhanced activity is repeated with each blade passage in this quadrant. In the more stable flow of Case B, the amplitude of the loading pattern is much reduced and generally symmetrical about the origin. While very strong, the loading peaks are confined to a single blade passage, suggesting the responsible disturbance was small but intense.

CONCLUSIONS

The distribution of alternating stresses at return frequencies of less than 100 cycles/h (referred to as the LCHA region) can be described as asymptotically decaying exponential for all critical loading areas with the exception of the blade root edgewise bending, where an extreme value distribution is appropriate. It is in the LCHA region that the maximum fatigue damage takes place. The shape or width parameters of each of these two parametric distributions are the most important and reflect the load response to varying operating conditions. We compared the accuracy of determining these parameters by fitting the target models to observed alternating cycle distributions determined by summing the results of 405, 10-minute time series and by counting the entire series as a single, concatenated record. We found that little was lost when the shape parameters were calculated from summing the load spectra from 405 individual 10-minute records versus counting them concatenated as a single record.

We believe that the asymptotic behavior observed in the LCHA load range is a consequence of the cycle counting process being Poisson. This means that, for record lengths or counting periods where stationarity can be assumed, the events (the closing of hysteresis stress/strain cycles) are independent of one another and

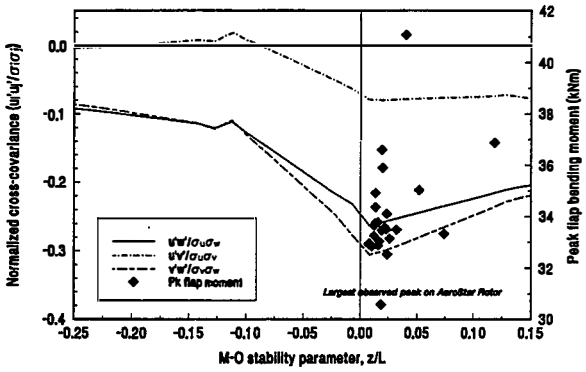

FIGURE 8. WIND COMPONENT NORMALIZED CROSS-COVARIANCE VERSUS STABILITY

their number depends only on the record length. We know that for atmospheric variables in a wind park environment, quasi-stationarity can only be achieved for periods near 10 minutes. Because the turbulence in the turbine inflow is the ultimate excitation of the observed load cycles, we stipulate that the process can be described as *nonhomogeneous* Poisson in which the scaling varies with time.

We determined the sensitivity of the distribution shape parameters to inflow fluid dynamics parameters by classifying the observed population of 10-minute records with respect to atmospheric stability and mean hub height horizontal wind speed. By cross-correlating several bulk measures of the turbulent inflow with the shape parameters, we determined that they were most sensitive to the stability and the mean shear stress measured at hub height. We also found that there is a narrow range of slightly stable flow conditions in which the distribution shape parameters reach their minimum (shallowest slope) indicating a broad range of load cycles are present. This stability range was also found to contain the highest values of the cross-covariances for the three wind components, indicating that the flow was dominated by highly correlated or coherent structures. It was also in this stability range where the majority of the 25 largest flapwise bending loads were observed in the Micon 65 data set.

We believe the conditions present in the narrow stability range discussed above support the existence of dynamic instability in the wind park flows. Under these conditions, small-scale perturbations such as those making up turbine wakes can grow exponentially with time. Also within the layer containing the turbine rotors, this range of stability can support the development of internal gravity waves and transient shear-generated phenomena such as Kelvin-Helmholtz instabilities. Observed evidence suggests that the disturbances responsible for the largest peak loads on the turbine rotors were of scales smaller than the rotor disk. These disturbances move vertically as well as horizontally through the disks.

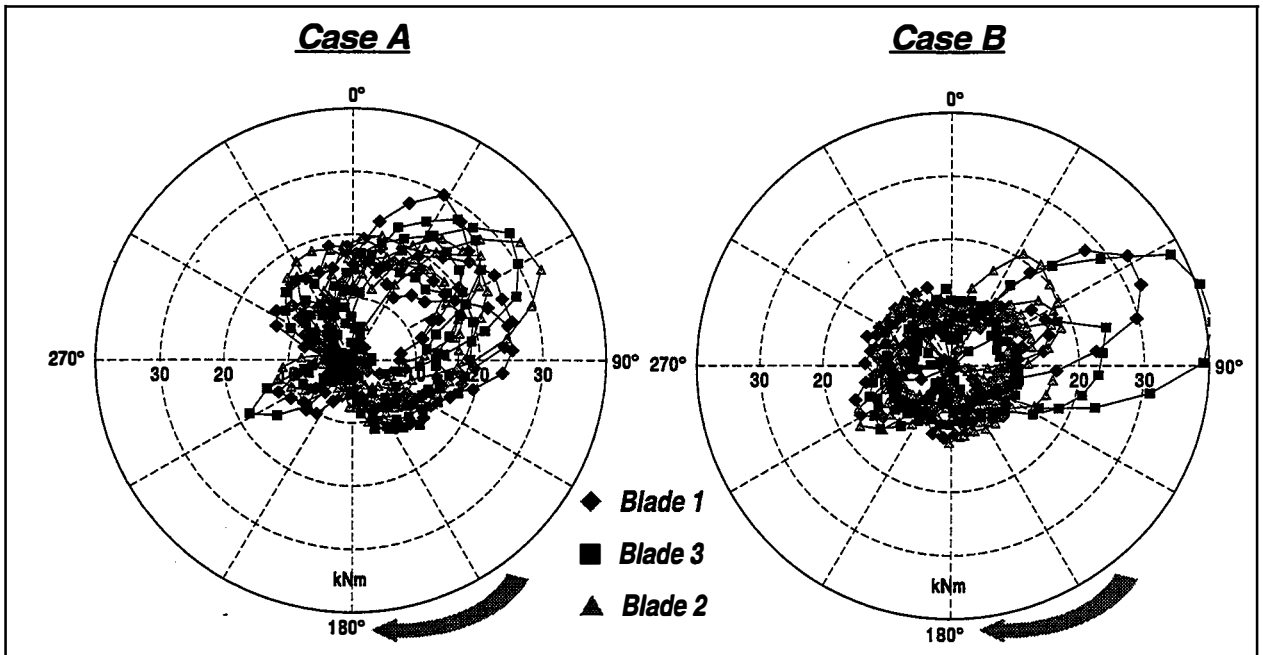

FIGURE 9. AZIMUTHAL POSITIONS OF PEAK FLAP LOADS OBSERVED ON NREL ROTOR

FUTURE WORK

In the limited space of this paper, we have concentrated on identifying the role of fluid dynamic parameters associated with the turbine inflow in influencing the observed load distributions in the important LCHA range. In the future, we will expand the work to document any impacts of site specificity and turbine design on the β_1 and γ_2 shape parameters. We will also explore methodologies to scale the amplitude parameters (β_0 , γ_1) of the distributions in Eqs.(1) and (2) and, if necessary, the position parameter, γ_0, of the extreme value distribution of edgewise root bending loads. Over the next two years, we hope to be able to repeat these measurements using a specific turbine design in a range of climates, as well as several different turbine designs in similar environments. By accomplishing these goals, we believe we can establish justifiable guidelines for aiding both the turbine designer and the project planner in mating the proper equipment to the desired operating environment.

ACKNOWLEDGMENTS

This work has been supported by the U.S. Department of Energy under contract number DE-AC02-83CH10093.

REFERENCES

[1] Kelley, N., Desrochers, G., Tangler, J., and Smith, B., October 1992, "A Discussion of the Results of the Rainflow Counting of a Wide Range of Dynamics Associated with the Simultaneous Operation of Adjacent Wind Turbines," NREL/TP-442-5159, National Renewable Energy Laboratory, Golden, CO.

[2] Kelley, N.D., June 1993, "Defining the Normal Turbine Inflow Within a Wind Park Environment," NREL/TP-442-5619, National Renewable Energy Laboratory, Golden, CO.

[3] Kelley, N.D., July 1993, "Inflow Characteristics Associated with High-Blade-Loading Events in a Wind Farm," NREL/TP-442-5623, National Renewable Energy Laboratory, Golden, CO.

[4] Jackson, K.L., July 1992, "Estimation of Fatigue Life Using Field Test Data," Oral Presentation to the NREL Wind Energy Program Subcontractor Review Meeting, Golden, CO.

[5] Tangler, J., Smith, B., Jager, D., and Olsen, T., September 1990, "Atmospheric Performance of the SERI Thin-Airfoil Family: Final Results," SERI/TP-257-3939, Solar Energy Research Institute, Golden, CO.

[6] Downing, S.D. and Socie, D.F., 1982, "Simple Rainflow Counting Algorithms," *Int. J. Fatigue*, Vol. 4(1).

[7] Sutherland, H.J. and Butterfield, C.P., 1994, "A Review of the Workshop on Fatigue Life Methodologies for Wind Turbines," *Proc. of 13th ASME ETCE Wind Energy Symposium*, W.D. Musial (ed), ASME, New Orleans, LA., January 1994.

[8] Roth, S.M., 1993, *Introduction to Probability Models,* Academic Press, Inc., San Diego, CA.

[9] Sutherland, H.J. and Osgood, R.M., October 1992, "Frequency Domain Synthesis of the Fatigue Load Spectrum for the NPS-100 Wind Turbine," *Proc. of WindPower '92*, AWEA, Washington, DC, pp. 321-328.

[10] Miles, J.W., 1961, "On the Stability of Heterogeneous Shear Flows," *J. Fluid Mech.*, Vol. 10., pp. 496-508.

[11] Drazin, P.G. and Reid, W.H., 1981, *Hydrodynamic Stability*, Cambridge Univ. Press, NY, NY, pp.320-458.